Paper: Rb15-2-01,1733xj 2832words

Method for Controlling Multi-DOF Ultrasonic Motor Using Neural Network

Kenjiro Takemura and Takashi Maeno

Dept. Mechanical Engineering, Keio University,
3-14-1, Hiyoshi, Kohoku-ku, Yokohama, 223-8522 Japan
E-mail: kenjiro@mmm-keio.net
[Received October 24, 2002; accepted December 5, 2002]

A multi-DOF ultrasonic motor developed by the authors can generate multi-DOF rotation of a spherical rotor using three orthogonal natural vibrations of a bar-shaped stator. The ultrasonic motor is suitable for making small, lightweight and simple multi-DOF motion unit. In the present paper, a control methodology for the multi-DOF ultrasonic motor is proposed and a motion control test using the method is conducted. First, we develop an inverse model of the multi-DOF ultrasonic motor using our prior knowledge of ultrasonic motors and neural network technique in order to deal with the redundancy and non-linearity of the driving characteristics. Second, we propose a novel control method using the inverse model. Then, numerical simulation and motion control test are conducted to confirm the ability of the proposed control method. The results confirm that the rotor can be rotated around arbitrary rotational axis using the inverse model, and that the proposed control method does work successfully.

Keywords: ultrasonic motor, multi-dof, control, neural network

1. Introduction

Recently, the number of DOFs for robot systems has increased as they have become used for various purposes. Now, we use the robots not only in industry field but also in medical, amusement and space fields etc. As the number of DOFs for the robots increase, we have problems on the number of actuators. The systems become huge and heavy. There can be two ways for engineers to solve this kind of problems. One is to make a small, high-power actuator with single-DOF motion. The other is to develop an actuator with several functions like multi-DOF actuator. The former is the extension of the present concept. Then, the system geometry and control scheme are kept to be the same as those of conventional system. On the other hand, if we take the latter, the new type of system configuration can be developed using the different concept from that of the conventional system. Hence, some multi-DOF actuators have been proposed and developed in last decades.

For examples of multi-DOF electromagnetic actuators, Roth et al. proposed a three-DOF variable-reluctance spherical wrist motor [1]. The motor provides three-DOF rotation of a spherical rotor using electromagnetic force. Yano et al. developed a spherical stepping motor and a synchronous motor with three-DOF [2,3]. Sokolov et al. developed a spherical direct drive actuator [4]. Ebara et al. presented a PM-type spherical motor [5]. Wang et al. reported a multi-DOF spherical magnet motor [6]. Furthermore, there also are studies on multi-DOF actuators using ultrasonic motors. Bansevicius reported a piezoelectric multi-DOF actuator [7]. Amano et al. developed an ultrasonic actuator with multi-DOF [8]. Aoyagi et al. constructed a multi-DOF ultrasonic motor using multimode ring-form vibrator [9]. Shimoda et al. reported an ultrasonic motor for driving spherical surface [10]. The actuators can provide multi-DOF motion using single stators, however, they cannot be used in place of multi-DOF motion units using several electromagnetic motors because of their complex structures, small output torque, difficulties in control, and so on.

According to the state of multi-DOF actuators as mentioned above, the authors have developed a multi-DOF ultrasonic motor [11,12]. The multi-DOF ultrasonic motor provides three-DOF rotation of a spherical rotor using three orthogonal natural vibration modes of a Langevin type vibrator (stator). In order to put the multi-DOF ultrasonic motor into practice, we construct a novel controller for the motor in this study. First, we construct an inverse model of the multi-DOF ultrasonic motor using prior knowledge about ultrasonic motors and neural network technique in order to deal with the redundant and non-linear characteristics of the motor. We call the model "knowledge-based inverse model." Lin et al. have already reported a neural network based inverse model of a single-DOF ultrasonic motor [13]. In their model, however, only single operating parameter is considered, because it is enough for controlling the motion of single-DOF ultrasonic motor. On the other hand, to fully express the motion of the multi-DOF ultrasonic motor, all potential operating parameters, adds up to six, must be considered. In our knowledge-based inverse model, all the parameters are considered. Second, a novel control method for multi-DOF ultrasonic motor using the knowledge-based inverse model is proposed. To confirm their effectiveness, we con-

duct numerical simulation and motion control tests of the rotor using the proposed control method.

2. Multi-DOF Ultrasonic Motor

We will briefly introduce you our prior studies about a multi-DOF ultrasonic motor in this section.

The multi-DOF ultrasonic motor we developed [11] is shown in **Fig.1**. The ultrasonic motor consists of a bar-shaped stator and a spherical rotor. The diameter, height, and mass of the stator are 10.0 mm, 31.8 mm, and 16.9 g, respectively. Multi-DOF rotation of the rotor like human wrist joint is generated using two bending vibrations and a longitudinal vibration of the stator, whose natural frequencies are designed to correspond. Basal driving principles of the ultrasonic motor are shown in **Fig.2**. The rotor is rotated around the *z*-axis by the rotor/stator frictional force, when the two orthogonal bending vibrations are excited on the stator with quarter cycle interval as shown in **Fig.2(a)**. On the other hand, the rotor is rotated around the *x*-(*y*-)axis, when the bending and longitudinal vibrations are combined as shown in **Fig.2(b)**. Furthermore, a rotation around arbitrary axis is generated when the vibrations are appropriately combined.

We have also developed a forward model of the multi-DOF ultrasonic motor [12]. Using the model, you can analyze the rotational axis, driving characteristics, and rotor/stator contact state of the motor under an arbitrary combination of the vibrations.

3. Inverse Model

The potential operating parameters of the multi-DOF ultrasonic motor are frequencies, amplitudes, and phases of three alternative inputs for generating three natural vibrations. Considering the driving principle, you can find that number of the independent parameters among them is six. Their combination is redundant with respect to an arbitrary rotational axis of the rotor. Furthermore, each parameter has non-linear characteristics against the rotational speed [12]. Namely, an inverse model for the input/output relation of the multi-DOF ultrasonic motor should be developed to realize the desired rotational axis. So, the inverse model is proposed using our prior knowledge about ultrasonic motors and neural network technique in this section.

3.1. Driving state representation

A representation method of driving state of the rotor is considered.

First, we define a rotational speed $\boldsymbol{N}$ to express the driving state. The direction and the magnitude of $\boldsymbol{N}$ represent the rotational axis and the rotational speed of the rotor, respectively. Each component represents the rotational speed around each axis of the reference frame in

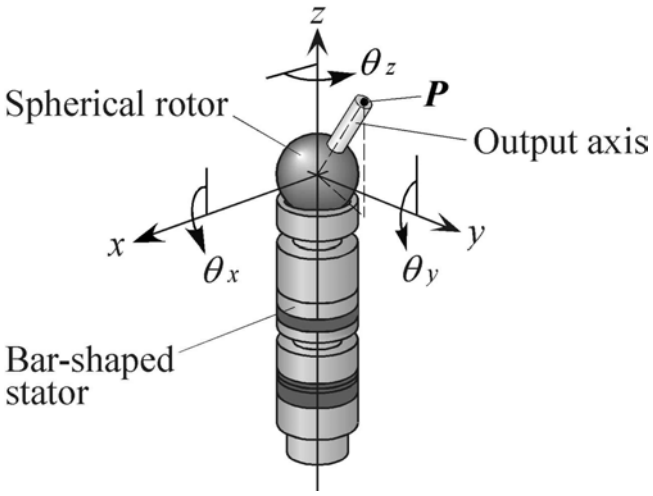

Fig. 1. Multi-DOF ultrasonic motor.

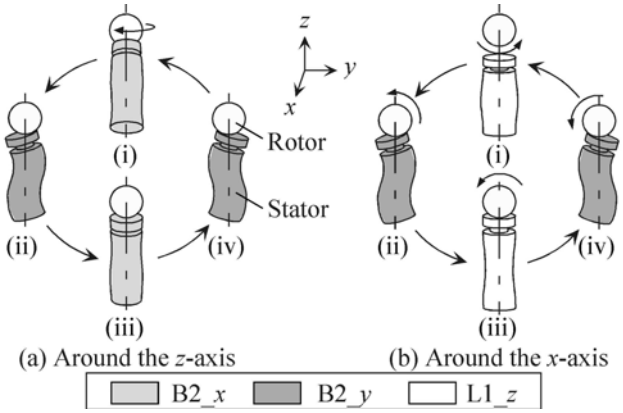

Fig. 2. Basal driving principle.

Fig.1.

Second, considering the driving principle of the multi-DOF ultrasonic motor (cf. **Fig.2**), a relative rotational speed $\boldsymbol{N}^r$ is defined as follows. The driving characteristics around the *x*- (*y*-) axis and *z*-axis are different each other depending on the driving principles. When rotor rotates around the *x*- (*y*-) axis, we use the driving principle of standing-wave type ultrasonic motor. On the other hand, when around the *z*-axis, we use that of traveling-wave type ultrasonic motor. So, we should scale $\boldsymbol{N}$ to the difference as,

$$N_\xi{}^r = \begin{cases} \dfrac{N_\xi}{N_{sta}^{xy}} & (\xi : x, y) \\ \dfrac{N_\xi}{N_{sta}^{z}} & (\xi : z) \end{cases} \quad \cdots\cdots\cdots\cdots (1)$$

Table 1. Phase relation and rotational direction.

Rotational axis	Phase [rad] ϕ_{B2x}	ϕ_{B2y}	ϕ_{L1z}	Rotational direction
x-axis	—	π/2	0	+ (CW)
	—	0	π/2	- (CCW)
y-axis	0	—	π/2	+ (CW)
	π/2	—	0	- (CCW)
z-axis	π/2	0	—	+ (CW)
	0	π/2	—	- (CCW)

where, $N_\xi{}^r$ is the *z*-component of a scaled rotational speed. ξ represents coordinates. N^{xy}_{sta} and N^{z}_{sta} are standard rotational speeds around the *x*- (*y*-) axis and the *z*-axis, respectively, which are obtained using the forward model of the multi-DOF ultrasonic motor developed in our previous study [12].

3.2. Classification of driving state

The diving state is expressed by $\boldsymbol{N}^r$ as mentioned above. The signs of each component of $\boldsymbol{N}^r$ represent the rotational directions. The rotational directions around the *x*-, *y*- and *z*-axis are related to phase differences of two combined vibrations as shown in **Table 1**. For example, the rotation around the *x*-axis should be CW when the bending vibration is in advance in phase with respect to the longitudinal vibration. So, we classify the driving state into eight categories according to the signs of each component of $\boldsymbol{N}^r$. The categories represent quadrant where $\boldsymbol{N}^r$ exists. Then, the phase relation between three vibrations is determined as **Table 2(i)**, while there still remains a certain range for each phase.

Our experiences in ultrasonic motors suggest the exact value of each phase. That is, the phase difference between the combined vibrations for the rotation around each axis should be quarter cycle in order to realize a high-performance motor. According to the knowledge, we determine that the phase difference between two vibrations related to maximum-value component of $\boldsymbol{N}^r$ is made to be quarter cycle, and that the relative amplitude $\boldsymbol{A}^r$ of the vibrations are to be 1.0. So, the driving state is still classified into three sub-categories considering the absolute value of components of $\boldsymbol{N}^r$. Then, the phases and relative amplitudes for two of three vibrations are exactly determined as in **Table 2(ii)**.

Still more, we must consider some special cases of driving states. The cases are when the rotational axis agrees with the *x*-, *y*- or *z*-axis, and when it exists in the *xy* plane. These cases are particularly classified from class 25 to class 28 as follows.

In the former cases, only the two vibrations are used to generate the rotation, and the phase difference between them is to be π/2 as shown in **Table 3**. Sub-class, "a" or "b", represents the sign of component.

In the latter case, the phase difference between the two bending vibrations is to be 0 or π, and that between bending and longitudinal vibrations is to be π/2 as shown in **Table 4**. Then, new-directional bending vibration and the longitudinal vibration are combined as the same way as **Fig.2(2)**.

Table 2. Classification of driving state.

	(i) Category			(ii) Sub-category				
class	cat.	N^r	Phase relation ●: *Ben_x* ●: *Ben_y* ○: *Lon_z*	sub-cat.	Maximum ingredient	Phase [rad] ϕ_{B2x} ϕ_{B2y} ϕ_{L1z}	Relative amplitude A^r_{B2x} A^r_{B2y} A^r_{L1z}
1	I	(+, +, -)	●—○—● ←π→	i	$\lvert N^r_x\rvert$	-π/2~0 π/2 0	A^r_x 1 1
2				ii	$\lvert N^r_y\rvert$	0 π/2~π π/2	1 A^r_y 1
3				iii	$\lvert N^r_z\rvert$	0 π/2 0~π/2	1 1 A^r_z
4	II	(+, -, +)	○—●—● ←π→	i	$\lvert N^r_x\rvert$	π/2~π π/2 0	A^r_x 1 1
5				ii	$\lvert N^r_y\rvert$	π/2 0~π/2 0	1 A^r_y 1
6				iii	$\lvert N^r_z\rvert$	π/2 0 -π/2~0	1 1 A^r_z
7	III	(+, -, -)	○—●—● ←π→	i	$\lvert N^r_x\rvert$	0~π/2 π/2 0	A^r_x 1 1
8				ii	$\lvert N^r_y\rvert$	π/2 π/2~π 0	1 A^r_y 1
9				iii	$\lvert N^r_z\rvert$	0 π/2 -π/2~0	1 1 A^r_z
10	IV	(-, +, +)	●—●—○ ←π→	i	$\lvert N^r_x\rvert$	0~π/2 0 π/2	A^r_x 1 1
11				ii	$\lvert N^r_y\rvert$	0 -π/2~0 π/2	1 A^r_y 1
12				iii	$\lvert N^r_z\rvert$	π/2 0 π/2~π	1 1 A^r_z
13	V	(-, +, -)	●—●—○ ←π→	i	$\lvert N^r_x\rvert$	-π/2~0 0 π/2	A^r_x 1 1
14				ii	$\lvert N^r_y\rvert$	0 0~π/2 π/2	1 A^r_y 1
15				iii	$\lvert N^r_z\rvert$	0 π/2 π/2~π	1 1 A^r_z
16	VI	(-, -, +)	●—○—● ←π→	i	$\lvert N^r_x\rvert$	π/2~π 0 π/2	A^r_x 1 1
17				ii	$\lvert N^r_y\rvert$	π/2 -π/2~0 0	1 A^r_y 1
18				iii	$\lvert N^r_z\rvert$	π/2 0 0~π/2	1 1 A^r_z
19	VII	(+, +, +)	●—●—● ←2π→	i	$\lvert N^r_x\rvert$	-π~-π/2 π/2 0	A^r_x 1 1
20				ii	$\lvert N^r_y\rvert$	0 -π~-π/2 π/2	1 A^r_y 1
21				iii	$\lvert N^r_z\rvert$	π/2 0 -π~-π/2	1 1 A^r_z
22	VIII	(-, -, -)	○—○—○ ←2π→	i	$\lvert N^r_x\rvert$	π/2~π -π/2 0	A^r_x 1 1
23				ii	$\lvert N^r_y\rvert$	0 π/2~π -π/2	1 A^r_y 1
24				iii	$\lvert N^r_z\rvert$	-π/2 0 π/2~π	1 1 A^r_z

Table 3. Phase relation when the rotational axis agrees with each frame axis.

class	sub-class	N^r	Phase [rad] ϕ_{B2x}	ϕ_{B2y}	ϕ_{L1z}	Relative amplitude A^r_{B2x}	A^r_{B2y}	A^r_{L1z}
25	a	(+, 0, 0)	0	π/2	0	0	1	1
	b	(-, 0, 0)	0	0	π/2			
26	a	(0, +, 0)	0	0	π/2	1	0	1
	b	(0, -, 0)	π/2	0	0			
27	a	(0, 0, +)	π/2	0	0	1	1	0
	b	(0, 0, -)	0	π/2	0			

Table 4. Phase relation when the rotational axis exists in *xy* plane.

class	sub-class	N^r	Phase [rad] ϕ_{B2x}	ϕ_{B2y}	ϕ_{L1z}	Relative amplitude A^r_{B2x}	A^r_{B2y}	A^r_{L1z}
28	a	(+, +, 0)	0	π	π/2	A^r_{B2x}	A^r_{B2y}	1
	b	(+, -, 0)	π/2	π/2	0			
	c	(-, +, 0)	0	0	π/2			
	d	(-, -, 0)	π/2	3π/2	0			

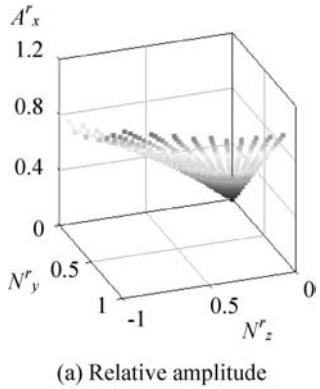

(a) Relative amplitude

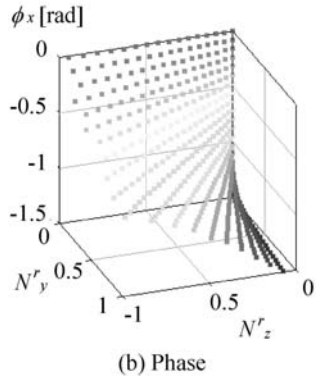

(b) Phase

Fig. 3. Non-linear characteristics of operating parameter.

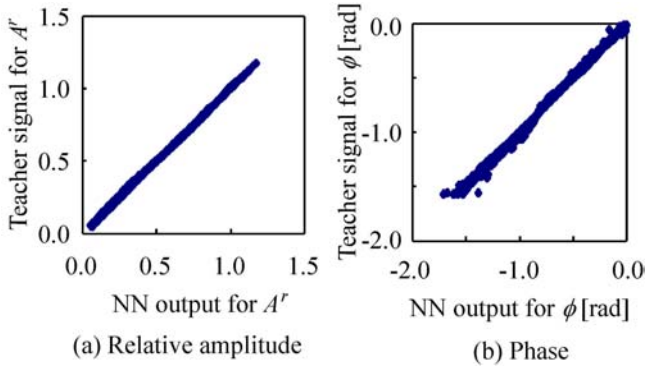

Fig. 4. Result of neural network training.

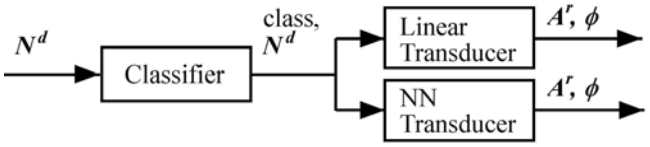

Fig. 5. Block diagram of inverse model.

According to the classification mentioned above, the driving state of rotor is divided into 28 classes. By the classification, the problems for the redundancy of operating parameters against the driving state is solved.

3.3. Non-linear Mapping

Two operating parameters, the phase and relative amplitude of one vibration, for class 1 to class 24 in Table 2 are still remained to be determined. Their exact values cannot be easily determined because they have non-linear characteristics against the driving state. For example, the characteristic between $\boldsymbol{N}^r$ and phase and that between $\boldsymbol{N}^r$ and amplitude of class 1 are shown in **Fig.3**. The characteristics are obtained by the forward model [12], where the relative amplitudes and phase difference of the vibrations related to x-component of $\boldsymbol{N}^r$ are 1.0 and $\pi/2$, respectively. According to the non-linearity, the neural network technique is used to map the characteristics. We use three-layer neural networks with two and one units respectively in sensory and response layers in order to map the characteristics of each parameter for each driving state. Sigmoid function is adopted in the units for the sensory and associate layers, and linear function is for the response layer. The sensory and associate layers have another unit for threshold.

For training the neural networks for each class, teacher signals are obtained using the forward model [12]. Connective weights of the neural networks are trained using the error back propagation method [13]. **Fig.4** shows the relationships between the teacher signals and outputs from trained neural network in case of class 1, where the training conditions are as follows: numbers of teacher signals, training cycle and units in associate layer are 1000, 30000 and 5, respectively. Initial connective weights are set to be random value between -3 and 3. A training rate is 0.5. The non-linear characteristics shown in **Fig.3** are well mapped after the training. The errors between the teacher signals and outputs are within 1.5 % of full scale. The neural networks for other classes are successfully trained as well.

3.4. Construction of Inverse Model

The inverse model of the multi-DOF ultrasonic motor is constructed using the above-mentioned classification and neural networks. **Fig.5** shows the block diagram of the inverse model. A classifier divides the desired rotational axis $\boldsymbol{N}^d$ into 28 classes. Then, according to the class, a linear transducer for class 25 to class 28 or a neural network transducer for class 1 to class 24 is alternatively used to provide the phases and relative amplitudes of three natural vibrations.

4. Control Method

4.1. Inverse Model Based Control

In this section, we propose a control method for the

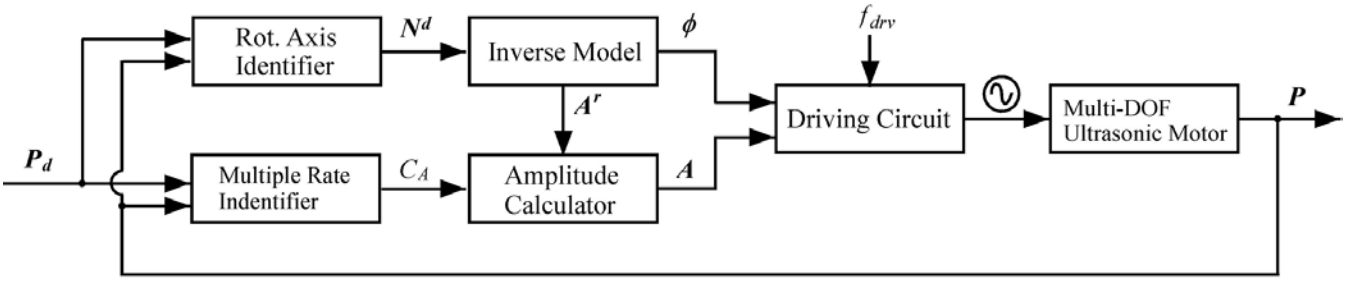

Fig. 6. Block diagram of control method.

multi-DOF ultrasonic motor using the inverse model. **Fig.6** shows the block diagram of the control method, where the control parameter $\boldsymbol{P}$ and the desired parameter $\boldsymbol{P_d}$ are the present and desired locations of the output axis in **Fig.1**, respectively. Each block plays the following roles.

Rotational Axis Identifier: A rotational axis identifier provides the desired rotational axis $\boldsymbol{N^d}$ using the following equation.

$$\boldsymbol{N^d} = \frac{\boldsymbol{P} \times \boldsymbol{P_d}}{|\boldsymbol{P} \times \boldsymbol{P_d}|} \quad \ldots\ldots\ldots\ldots\ldots\ldots\ldots\ldots (2)$$

Inverse Model: The inverse model determines the phases $\boldsymbol{\phi}$ and relative amplitudes $\boldsymbol{A^r}$ of three alternating inputs for the multi-DOF ultrasonic motor (*cf.* section 3).

Multiple Rate Identifier: A multiple rate identifier provides the multiple rate C_A of amplitudes for three alternating inputs. For example, it is constructed using the proportional control algorithm as follows.

$$\begin{cases} C_A = K_p \cdot \Delta\theta \\ \Delta\theta = \cos^{-1}\dfrac{|\boldsymbol{P} \cdot \boldsymbol{P_d}|}{|\boldsymbol{P}|\,|\boldsymbol{P_d}|} \end{cases} \quad \ldots\ldots\ldots\ldots\ldots\ldots (3)$$

where K_p is the proportional feedback again, and $\Delta\theta$ is the angle between $\boldsymbol{P}$ and $\boldsymbol{P_d}$.

Amplitude Calculator: An amplitude calculator determines the amplitudes $\boldsymbol{A}$ of three alternating inputs from the relative amplitudes $\boldsymbol{A^r}$ and the multiple rate C_A using the following equation.

$$\boldsymbol{A} = C_A \times \boldsymbol{A^r} \quad \ldots\ldots\ldots\ldots\ldots\ldots\ldots\ldots (4)$$

Driving Circuit: The blocks mentioned above determine the phases and amplitudes of three inputs. The driving circuit provides three alternating voltages according to the decided parameters, while the driving frequencies f_{drv} of the inputs are set to be equal to the corresponded natural frequencies f_0 of three vibrations used in the multi-DOF ultrasonic motor.

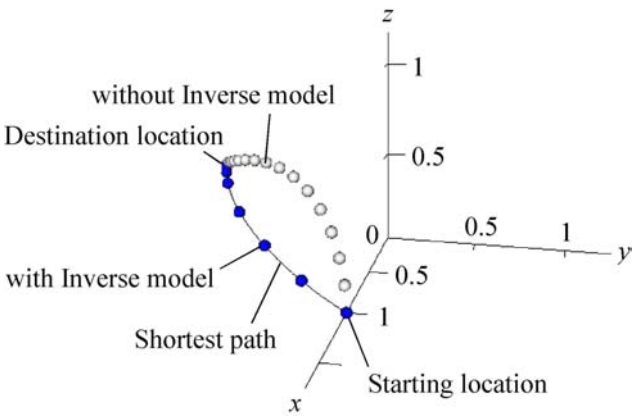

Fig. 7. Simulated result of step response.

4.2. Numerical Simulation on Inverse Model Based Control

In order to confirm the effectiveness of the inverse model based control method, we conduct a numerical simulation on a step response of a location of the output axis $\boldsymbol{P}$ shown in **Fig.1**. For comparison, the location of the output axis $\boldsymbol{P}$ is also controlled as a combination of the rotation around the *x*- and *y*-axis in series. The starting and destination locations of $\boldsymbol{P}$ are (1.00, 0.00, 0.00) and (0.29, -0.83, 0.48), respectively. **Fig.7** shows the history plot of $\boldsymbol{P}$ It can be seen that the location of $\boldsymbol{P}$ moves on the shortest path between the staring/destination locations only when the inverse model is used. It is because of that the position declination of $\boldsymbol{P}$ can be spatially considered only when the inverse model is used. So, we confirm the effectiveness of the proposed control method.

5. Experiment

An experiment for controlling the location of the output axis $\boldsymbol{P}$ is performed using the proposed control method. **Fig.8** shows the experimental setup. The setup is constructed as a master-slave system. The joystick (Microsoft SideWinder) is used as a master device to present the desired location of the output axis $\boldsymbol{P_d}$. The location of the output axis $\boldsymbol{P}$ is measured using potentiometers as shown in **Fig.8**. The controller is implemented on a personal computer.

Figure 9 shows an experimental result, where the driv-

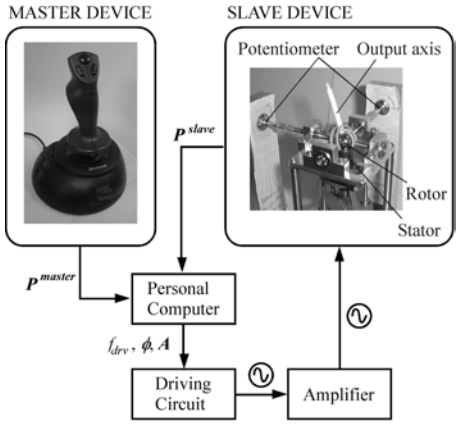

Fig. 8. Experimental setup.

ing frequency *fdrv* and maximum input voltage are 39.8 kHz and 24 V, respectively. **Fig.9(a)** shows the history plot of ***P***, and **Fig.9(b)** shows the history of the driving class (cf. **Table 2, 3** and **4**). The location ***P*** of the slave device successfully follows that of the master device using the inverse model based controller as shown in **Fig.9(a)**. During the control, it is also seen from **Fig.9(b)** that the driving class is successfully switched in the inverse model.

The control method using the proposed inverse model can be used not only for our motor but also for the other multi-DOF ultrasonic motors [7-9].

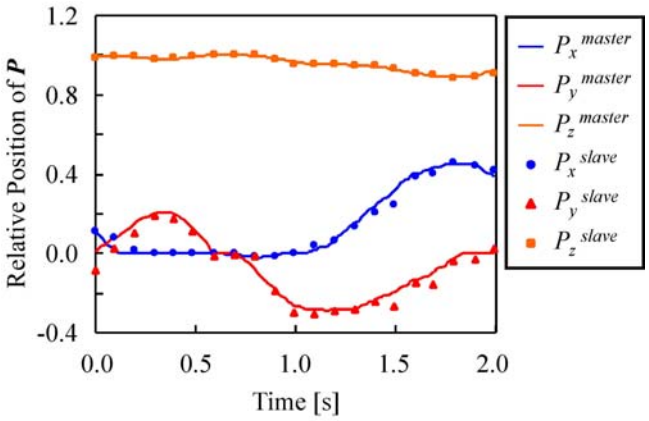

(a) History plot of the location of output axis

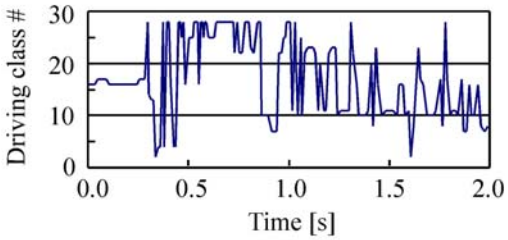

(b) History of driving class

Fig. 9. Experimental result for motion control test.

6. Conclusions

The control method of the multi-DOF ultrasonic motor is developed in the present study. First, the inverse model of the multi-DOF ultrasonic motor is constructed. The inverse model successfully provides the input parameters for the ultrasonic motor with respect to the desired rotational axis of the rotor. In other word, the inverse model makes the spherical rotor possible to rotate around an arbitrary rotational axis. It is clarified from the process of constructing the inverse model that the problems of the redundant and non-linear characteristics of the multi-DOF ultrasonic motor are solved using our prior knowledge of ultrasonic motors and neural network technique. Second, the control method is proposed using the inverse model. The location of output axis of the rotor can be controlled to the desired point using the control method. Finally, effectiveness of the proposed control method is confirmed both by the numerical simulation and experiment.

Future study focuses on applying the multi-DOF ultrasonic motor including controller to an active endoscope and multi-DOF robots. The inverse model and control method did work as mentioned in this paper, however, transitional characteristics have not been clarifyed yet. If it is necessary to know the transitional characteristics, we should refine the inverse model as to express the dynamic characteristics.

Acknowledgment
This research was supported in part by Canon Inc.

References:

[1] Roth, R. B. and Lee, K.-M., "Design Opimization of a Three Degrees-of-Freedom Variable-Reluctance Spherical Wrist Motor," Trans. ASME J. Engineering for Industry, Vol. 117, pp. 378-388, 1995.

[2] Yano, T., Suzuki, T., Sonoda, M. and Kaneko, M., "Basic Characteristics of the Developed Spherical Stepping Motor," Proc. 1999 IEEE/RSJ Int. Conf. Intelligent Robots and Systems, Vol. 3, pp. 1393-1398, 1999.

[3] Yano, T., Kaneko, M. and Sonoda, M., "Development of a Synchronous Motor With Three Degrees of Freedom," Proc. Theory and Practice of Robots and Manipulators 10:The 10th CISM-IFToMM Symposium, Vol. 2, 1997.

[4] Sokolov, S. M., Trifonov, O. V. and Yaroshevsky, V. S., "Research of Spherical Derect Drive Actuators Control System," Proc. 2001 IEEE International Conference on Robtics and Automation, pp. 1780-1785, 2001.

[5] Ebara, D., Katsuyama, N. and Kajioka, M., "Research of Spherical Derect Drive Actuators Control System," Proc. 2001 IEEE International Conference on Robtics and Automation, pp. 1792-1797, 2001.

[6] Wang, J., Mitcell, K., Jewell, G. W., and Howe, D., "Multi-Degree-of-Freedom Spherical Magnet Motors," Proc. 2001 IEEE International Conference on Robtics and Automation, pp. 1798-1805, 2001.

[7] Bansevicius, R., "Piezoelectric Multi-Degree-of-Freedom Actuators/Sensors,"Proc. 3rd Int. Conf. Motion and Vibration, pp. K9-K15, 1996.
[8] Amano, T., Ishii, T., Nakamutra, K. and Ueha, S., "An Ultrasonic Actuator with Multi-degree of Freedom Using Bending and longitudinal Vibrations of a sSingle Stator,"Proc. IEEE Ultrasonics Symposium, Vol. 1, pp. 667-670, 1998.
[9] Aoyagi, M., Tomikawa, Y. and Takano, T., "Construction of Multi-Degree-of-Freedom Ultrasonic Motor using Multi-mode Ring-form Vibrator,"Proc. 1999 Spring Meetng of the Acoustical Society of Japan, Vol. II, pp. 979-980, 1999.
[10] Shimoda, S., Ueyama, M., Matsuda, S., Matsuo, T., Sasaki, K. and Itao, K., "Design of Ultrasonic Motor for Driving Spherical Surface,"Proc. Int. Conf. Machine Automation 2000, pp. 255-260, 2000.
[11] Takemura, K. and Maeno, T., "Design and Control of an Ultrasonic Motor Capable of Generating Multi-DOF Motion,"IEEE/ASME Trans. Mechatronics, Vol. 6, No. 4, pp. 499-506, 2001.
[12] Takemura, K. and Maeno, T., "Numerical Analyses on Multi-DOF Ultrasonic Motor - Development of Analysis Method and Results -,"Proc. IEEE Int. Conf. Robotics and Automation, pp. 2387-2392, 2002.
[13] Lin, F.-J., Wai, R.-J. and Wang, S.-L., "A Fuzzy Neural Network Controller for Parallel-Resonant Ultrasonic Motor Drive,"IEEE Trans. Industry Electronics, Vol. 45, No. 6, pp. 928-937, 1998.

Name:
Kenjiro Takemura

Affiliation:
Research Associate, Department of Mechanical Engineering, Keio University

Address:
3-14-1, Hiyoshi, Kohoku-ku, Yokohama, 223-8522 Japan

Brief Biographical History:
2001- Research Fellow of Japan Society of Promotion of Science
2002- Research Associate at Keio University

Main Works:
- "Design and control of an Ultrasonic Motor Capable of Generating Multi-DOF Motion," IEEE/ASME Trans. Mechatronics, Vol. 6, No. 4, pp. 499-506 (2001)

Membership in Learned Societies:
- The Japan Society of Mechanical Engineering (JSME)
- The Robotics Society of Japan (RSJ)
- The Acousticsl Society of Japan (ASJ)

Name:
Takashi Maeno

Affiliation:
Associate Professor, Department of Mechanical Engineering, Keio University

Address:
3-14-1, Hiyoshi, Kohoku-ku, Yokohama, 223-8522 Japan

Brief Biographical History:
1986- Canon, Inc.
1995- Assistant Professor at Keio University
1999- Associate Professor at Keio University

Membership in Learned Societies:
- The Japan Society of Mechanical Engineers (JSME)
- The Robotics Society of Japan (RSJ)
- The Japanese Society of Instrumentation and Control Engineers (SICE)